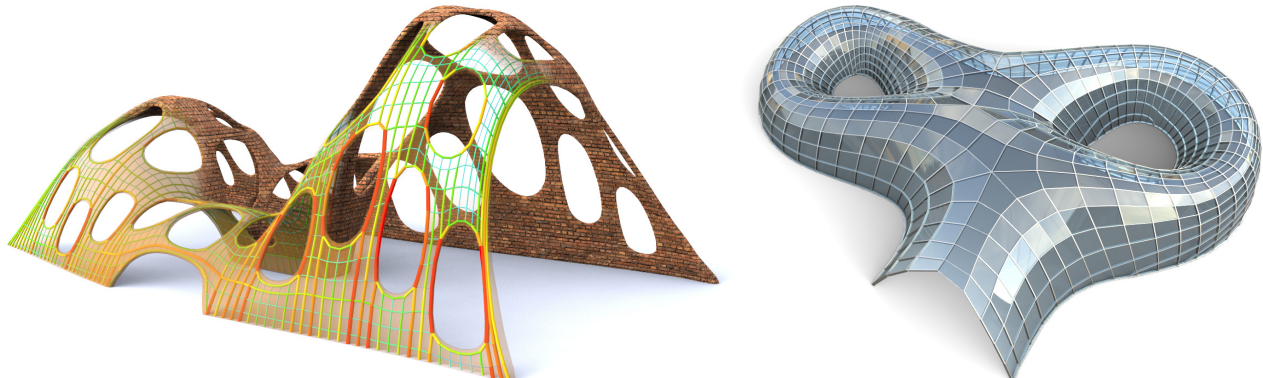


# Design of Self-supporting Surfaces



**Figure 1:** Left: Surfaces with irregularly placed holes are hard to realize as masonry, where the mortar between bricks must not be subject to tensile stresses. The surface shown here, surprisingly, has this property – it has been found as the nearest self-supporting shape from a given freeform geometry. The fictitious thrust network used in our algorithms is superimposed, with edges’ cross-section and coloring visualizing the magnitude of forces (warmer colors represent higher stresses.) Right: Curvature analysis with respect to the Airy stress surface tells us how to remesh shapes by self-supporting quad meshes with planar faces. This guides steel/glass constructions with low moments in nodes.

## Abstract

Self-supporting masonry is one of the most ancient and elegant techniques for building curved shapes. Because of the very geometric nature of their failure, analyzing and modeling such structures is more a geometry processing problem than one of classical continuum mechanics. This paper uses the thrust network method of analysis and presents an iterative nonlinear optimization algorithm for efficiently approximating freeform shapes by self-supporting ones. The rich geometry of thrust networks leads us to close connections between diverse topics in discrete differential geometry, such as a finite-element discretization of the Airy stress potential, perfect graph Laplacians, and computing admissible loads via curvatures of polyhedral surfaces. This geometric viewpoint allows us, in particular, to remesh self-supporting shapes by self-supporting quad meshes with planar faces, and leads to another application of the theory: steel/glass constructions with low moments in nodes.

**CR Categories:** I.3.5 [Computer Graphics]: Computational Geometry and Object Modeling—Curve, surface, solid, and object representations;

**Keywords:** Discrete differential geometry, architectural geometry, self-supporting masonry, thrust networks, reciprocal force diagrams, discrete Laplacians, isotropic geometry, mean curvature

## 1 Introduction

Vaulted masonry structures are among the simplest and at the same time most elegant solutions for creating curved shapes in building construction. For this reason they have been an object of interest since antiquity: large, non-convex examples of such structures include gothic cathedrals. They continue to be an active topic of research today.

Our paper is concerned with a combined geometry+statics analysis of *self-supporting* masonry and with tools for the interactive modeling of freeform self-supporting structures. Here “self-supporting” means that the structure, considered as an arrangement of blocks

(bricks, stones), holds together by itself, with additional support present only during construction. This analysis is based on the following assumptions, which follow the classic [Heyman 1966]:

*Assumption 1:* Masonry has no tensile strength, but the individual building blocks do not slip against each other (because of friction or mortar). On the other hand, their compressive strength is sufficiently high so that failure of the structure is by a sudden change in geometry and not by material failure.

*Assumption 2 (The Safe Theorem):* If a system of forces can be found which is in equilibrium with the load on the structure and which is contained within the masonry envelope then the structure will carry the loads, although the actual forces present may not be those postulated by that system.

Our approach is twofold: We first give an overview of the continuous case of a smooth surface under stress, which turns out to be governed locally by the Airy stress function. This mathematical model is called a membrane in the engineering literature and has been applied to the analysis of masonry before. The surface is self-supporting if and only if stresses are entirely compressive. For computational purposes, stresses are discretized as a fictitious *thrust network* [Block and Ochsendorf 2007] contained in the masonry structure; this network is a system of forces in equilibrium with the structure’s deadload. It can be interpreted as a finite element discretization of the continuous case, and it turns out to have very interesting geometry, with the Airy stress function becoming a polyhedral surface directly related to a reciprocal force diagram.

While previous work in architectural geometry was mostly concerned with aspects of rationalization and purely geometric side-conditions which occur in freeform architecture, the focus of this paper is design with *statics* constraints. In particular, our contributions are the following:

**Contributions.** • We present an optimization algorithm, based on the theory of thrust networks and Airy potentials, for efficiently finding a self-supporting surface near a given arbitrary reference surface (§3), and build a tool for interactive design of self-supporting surfaces based on this algorithm (§4). Freeform masonry is based on such surfaces.

71 • The discrete “stress Laplacian” derived from a thrust network  
 72 with compressive forces is a so-called perfect one (§2.2). We use it  
 73 to argue why our discretizations are faithful to the continuous case.

74 • We connect the physics of self-supporting surfaces with the ge-  
 75 ometry of isotropic 3-space, and express the equations governing  
 76 self-supporting surfaces in terms of curvatures (§2.3) and (§2.4).  
 77 Likewise we establish a connection between the stress Laplacian  
 78 and mean curvatures of polyhedral surfaces. This theoretical part  
 79 of the paper is a contribution to Discrete Differential Geometry.

80 • We use the geometric knowledge we have gathered to find par-  
 81 ticularly nice families of self-supporting surfaces, especially planar  
 82 quadrilateral representations of thrust networks (§5). This leads to  
 83 steel/glass structures with low bending and torsion moments.

84 **Related Work.** Unsupported masonry has been an active topic of  
 85 research in the engineering community. The foundations for the  
 86 modern approach were laid by Jacques Heyman [1966] and are  
 87 available as the textbook [Heyman 1995]. The theory of reciprocal  
 88 force diagrams in the planar case was studied by Maxwell [Maxwell  
 89 1864]; a unifying view on polyhedral surfaces, compressive forces  
 90 and corresponding “convex” force diagrams is presented by [Ash  
 91 et al. 1988]. F. Fraternali [2002; 2010] established a connection  
 92 between the continuous theory of stresses in membranes and the  
 93 discrete theory of forces in thrust networks, by interpreting the lat-  
 94 ter as a non-conforming finite element discretization of the former.

95 Several authors have studied the problem of finding discrete com-  
 96 pressive force networks contained within the boundary of masonry  
 97 structures; previous work in this area includes [O’Dwyer 1998]  
 98 and [Andreu et al. 2007]. Fraternali [2010] proposed solving for  
 99 the structure’s discrete stress surface, and examining its convex  
 100 hull to study the structure’s stability and susceptibility to cracking.  
 101 Philippe Block’s seminal thesis introduced *Thrust Network Analysis*,  
 102 which pioneered the use of thrust networks and their reciprocal  
 103 diagrams for efficient and practical design of self-supporting ma-  
 104 sonry structures. By first seeking a reciprocal diagram of the top  
 105 view, guaranteeing equilibrium of horizontal forces, then solving  
 106 for the heights that balance the vertical loads, Thrust Network An-  
 107 alysis linearizes the form-finding problem. For a thorough overview  
 108 of this methodology, see e.g. [Block and Ochsendorf 2007; Block  
 109 2009]. Recent work by Block and coauthors extends this method  
 110 in the case where the reciprocal diagram is not unique; for different  
 111 choices of reciprocal diagram, the optimal heights can be found us-  
 112 ing the method of least squares [Van Mele and Block 2011], and the  
 113 search for the best such reciprocal diagram can be automated using  
 114 a genetic algorithm [Block and Lachauer 2011].

115 Other approaches to the design of self-supporting structures include  
 116 modeling these structures as damped particle-spring systems [Kil-  
 117 ian and Ochsendorf 2005; Barnes 2009], and mirroring the rich  
 118 tradition in architecture of designing self-supporting surfaces us-  
 119 ing hanging chain models [Heyman 1998]. Alternatively, masonry  
 120 structures can be represented by networks of rigid blocks [Livesley  
 121 1992], whose conditions on the structural feasibility were incorpo-  
 122 rated into procedural modeling of buildings [Whiting et al. 2009].

123 Algorithmic and mathematical methods relevant to this paper are  
 124 work on the geometry of PQ meshes [Liu et al. 2006], discrete  
 125 curvatures for such meshes [Pottmann et al. 2007; Bobenko et al.  
 126 2010], in particular curvatures in isotropic geometry [Pottmann and  
 127 Liu 2007]. Schiftner and Balzer [2010] discuss approximating a  
 128 reference surface by a quad mesh with planar faces, whose layout  
 129 is guided by statics properties of that surface.

## 2 Self-supporting Surfaces

This section contains the theoretical basis of the paper. §2.1 and §2.2 explain the mathematical model for unsupported masonry and the discretization needed in our algorithms. The connection with isotropic geometry (§2.3 and §2.4) is important for the later Section 5, which deals with self-supporting PQ (planar quad) meshes and moment-free steel/glass constructions. Finally we discuss convergence (§2.5).

### 2.1 The Continuous Theory

We model masonry as a surface given by a height field  $s(x, y)$  de-  
 fined in some planar domain  $\Omega$ . We assume that there are vertical  
 loads  $F(x, y)$  — usually  $F$  represents the structure’s own weight.  
 By definition this surface is self-supporting if and only if there ex-  
 ists a field of compressive stresses which are in equilibrium with  
 the acting forces. This is equivalent to existence of a field  $M(x, y)$   
 of  $2 \times 2$  symmetric positive semidefinite matrices satisfying

$$\operatorname{div}(M\nabla s) = F, \quad \operatorname{div} M = 0, \quad (1)$$

where the divergence operator  $\operatorname{div} \begin{pmatrix} u(x,y) \\ v(x,y) \end{pmatrix} = u_x + v_y$  is under-  
 stood to act on the columns of a matrix (see e.g. [Fraternali 2010],  
 [Giaquinta and Giusti 1985]).

The condition  $\operatorname{div} M = 0$  says that  $M$  is locally the Hessian of a  
 real-valued function  $\phi$  (the *Airy stress potential*): With the notation

$$M = \begin{pmatrix} m_{11} & m_{12} \\ m_{12} & m_{22} \end{pmatrix} \iff \widehat{M} = \begin{pmatrix} m_{22} & -m_{12} \\ -m_{12} & m_{11} \end{pmatrix}$$

it is clear that  $\operatorname{div} M = 0$  is an integrability condition for  $\widehat{M}$ , so  
 locally there is a potential  $\phi$  with

$$\widehat{M} = \nabla^2 \phi, \quad \text{i.e.,} \quad M = \widehat{\nabla^2 \phi}.$$

If the domain  $\Omega$  is simply connected, this relation holds globally.  
 Positive semidefiniteness of  $M$  (or equivalently of  $\widehat{M}$ ) character-  
 izes *convexity* of the Airy potential  $\phi$ . The Airy function enters  
 computations only by way of its derivatives, so global existence is  
 not an issue.

*Remark:* Stresses at boundary points depend on the way the sur-  
 face is anchored: A fixed anchor means no condition, but a free  
 boundary with outer normal vector  $\mathbf{n}$  means  $\langle M\nabla s, \mathbf{n} \rangle = 0$ .

**Stress Laplacian.** Note that  $\operatorname{div} M = 0$  yields  $\operatorname{div}(M\nabla s) =$   
 162  $\operatorname{tr}(M\nabla^2 s)$ , which we like to call  $\Delta_\phi s$ . The operator  $\Delta_\phi$  is sym-  
 163 metric. It is elliptic (as a Laplace operator should be) if and only if  
 164  $M$  is positive definite, i.e.,  $\phi$  is strictly convex. The balance condi-  
 165 tion (1) may be written as  $\Delta_\phi s = F$ .

### 2.2 Discrete Theory: Thrust Networks

We discretize a self-supporting surface by a mesh  $\mathcal{S} = (V, E, F)$   
 (see Figure 2). Loads are again vertical, and we discretize them as  
 force densities  $F_i$  associated with vertices  $\mathbf{v}_i$ . The load acting on  
 this vertex is then given by  $F_i A_i$ , where  $A_i$  is an area of influence  
 (using a prime to indicate projection onto the  $xy$  plane,  $A_i$  is the  
 area of the Voronoi cell of  $\mathbf{v}'_i$  w.r.t.  $V'$ ). We assume that stresses  
 are carried by the edges of the mesh: the force exerted on the vertex  
 $\mathbf{v}_i$  by the edge connecting  $\mathbf{v}_i, \mathbf{v}_j$  is given by

$$w_{ij}(\mathbf{v}_j - \mathbf{v}_i), \quad \text{where} \quad w_{ij} = w_{ji} \geq 0.$$

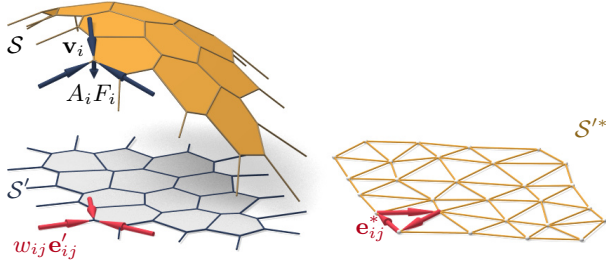


**Figure 2:** A thrust network  $\mathcal{S}$  with dangling edges indicating external forces (left). This network together with compressive forces which balance vertical loads  $A_i F_i$  projects onto a planar mesh  $\mathcal{S}'$  with equilibrium compressive forces  $w_{ij} \mathbf{e}'_{ij}$  in its edges. Rotating forces by 90° leads to the reciprocal force diagram  $\mathcal{S}'^*$  (right).

175 The nonnegativity of the individual weights  $w_{ij}$  expresses the  
176 compressive nature of forces. The balance conditions at vertices then  
177 read as follows: With  $\mathbf{v}_i = (x_i, y_i, s_i)$  we have

$$\sum_{j \sim i} w_{ij}(x_j - x_i) = \sum_{j \sim i} w_{ij}(y_j - y_i) = 0, \quad (2)$$

$$\sum_{j \sim i} w_{ij}(s_j - s_i) = A_i F_i. \quad (3)$$

188 A mesh equipped with edge weights in this way is a discrete *thrust network*. Invoking the safe theorem, we can state that a masonry structure is self-supporting, if we can find a thrust network with compressive forces which is entirely contained within the structure.

182 **Reciprocal Diagram.** Equations (2) have a geometric interpretation: with edge vectors

$$\mathbf{e}'_{ij} = \mathbf{v}'_j - \mathbf{v}'_i = (x_j, y_j) - (x_i, y_i),$$

184 Equation (2) asserts that vectors  $w_{ij} \mathbf{e}'_{ij}$  form a closed cycle. Rotating them by 90 degrees, we see that likewise

$$\mathbf{e}'^*_{ij} = w_{ij} J \mathbf{e}'_{ij}, \quad \text{with } J = \begin{pmatrix} 0 & -1 \\ 1 & 0 \end{pmatrix},$$

186 form a closed cycle (see Figure 2). If the mesh  $\mathcal{S}$  is simply connected, there exists an entire *reciprocal diagram*  $\mathcal{S}'^*$  which is a  
187 combinatorial dual of  $\mathcal{S}$ , and which has edge vectors  $\mathbf{e}'^*_{ij}$ . Its  
188 vertices are denoted by  $\mathbf{v}'^*_i$ .

190 *Remark:* If  $\mathcal{S}'$  is a Delaunay triangulation, then the corresponding  
191 Voronoi diagram is an example of a reciprocal diagram.

192 **Polyhedral Stress Potential.** We can go further and construct a  
193 convex polyhedral “Airy stress potential” surface  $\Phi$  with vertices  
194  $\mathbf{w}_i = (x_i, y_i, \phi_i)$  combinatorially equivalent to  $\mathcal{S}$  by requiring that  
195 a primal face of  $\Phi$  lies in the plane  $z = \alpha x + \beta y + \gamma$  if and only if  
196  $(\alpha, \beta)$  is the corresponding dual vertex of  $\mathcal{S}'^*$  (see Figure 3). Ob-  
197 viously this condition determines  $\Phi$  up to vertical translation. For  
198 existence see [Ash et al. 1988]. The inverse procedure constructs  
199 a reciprocal diagram from  $\Phi$ . This procedure works also if forces  
200 are not compressive: we can construct an Airy mesh  $\Phi$  which has  
201 planar faces, but it will no longer be a convex polyhedron.

202 The vertices of  $\Phi$  can be interpolated by a piecewise-linear function  
203  $\phi(x, y)$ . It is easy to see that the derivative of  $\phi(x, y)$  jumps by the  
204 amount  $\|\mathbf{e}'^*_{ij}\| = w_{ij} \|\mathbf{e}'_{ij}\|$  when crossing over the edge  $\mathbf{e}'_{ij}$  at right  
205 angle, with unit speed. This identifies  $\Phi$  as the Airy polyhedron in-  
206 troduced by [Fraternali et al. 2002] as a finite element discretization  
207 of the continuous Airy function (see also [Fraternali 2010]).

208 If the mesh is not simply connected, the reciprocal diagram and  
209 the Airy polyhedron exist only locally. Our computations do not  
210 require global existence.

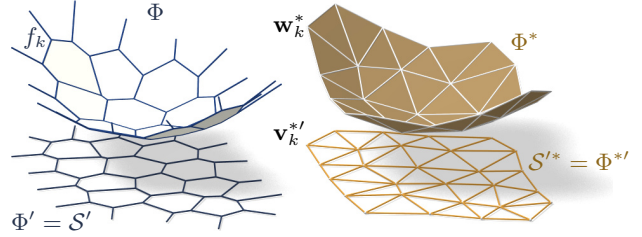


**Figure 3:** Airy stress potential  $\Phi$  and its polar dual  $\Phi^*$ .  $\Phi$  projects onto the same planar mesh as  $\mathcal{S}$  does, while  $\Phi^*$  projects onto the reciprocal force diagram. A primal face  $f_k$  lies in the plane  $z = \alpha x + \beta y + \gamma \iff$  the corresponding dual vertex is  $\mathbf{w}_k^* = (\alpha, \beta, -\gamma)$ .

211 **Polarity.** Polarity with respect to the Maxwell paraboloid  $z =$   
212  $\frac{1}{2}(x^2 + y^2)$  maps the plane  $z = \alpha x + \beta y + \gamma$  to the point  $(\alpha, \beta, -\gamma)$ .  
213 Thus, applying polarity to  $\Phi$  and projecting the result  $\Phi^*$  into the  $xy$   
214 plane reconstructs the reciprocal diagram  $\Phi'^* = \mathcal{S}'^*$  (see Fig. 3).

215 **Discrete Stress Laplacian.** The weights  $w_{ij}$  may be used to de-  
216 fine a graph Laplacian  $\Delta_\phi$  which on vertex-based functions acts as

$$\Delta_\phi s(\mathbf{v}_i) = \sum_{j \sim i} w_{ij}(s_j - s_i).$$

217 This operator is a perfect discrete Laplacian in the sense of [War-  
218 detzky et al. 2007], since it is symmetric by construction, Equa-  
219 tion (2) implies linear precision for the planar “top view mesh”  $\mathcal{S}'$   
220 (i.e.,  $\Delta_\phi f = 0$  if  $f$  is a linear function), and  $w_{ij} \geq 0$  ensures  
221 semidefiniteness and a maximum principle for  $\Delta_\phi$ -harmonic func-  
222 tions. Equation (3) can be written as  $\Delta_\phi s = AF$ .

223 Note that  $\Delta_\phi$  is well defined even when the underlying meshes are  
224 not simply connected.

### 2.3 Surfaces in Isotropic Geometry

226 It is worthwhile to reconsider the basics of self-supporting surfaces  
227 in the language of dual-isotropic geometry, which takes place in  $\mathbb{R}^3$   
228 with the  $z$  axis as a distinguished vertical direction. The basic ele-  
229 ments of this geometry are planes, having equation  $z = f(x, y) =$   
230  $\alpha x + \beta y + \gamma$ . The gradient vector  $\nabla f = (\alpha, \beta)$  determines the  
231 plane up to translation. A plane tangent to the graph of the function  
232  $s(x, y)$  has gradient vector  $\nabla s$ .

233 There is the notion of *parallel points*:  $(x, y, z) \parallel (x', y', z') \iff$   
234  $x = x', y = y'$ .

235 *Remark:* The Maxwell paraboloid is considered the unit sphere of  
236 isotropic geometry, and the geometric quantities considered above  
237 are assigned specific meanings: The forces  $\|\mathbf{e}'^*_{ij}\| = w_{ij} \|\mathbf{e}'_{ij}\|$  are  
238 dihedral angles of the Airy polyhedron  $\Phi$ , and also “lengths” of  
239 edges of  $\Phi^*$ . We do not use this terminology in the sequel.

240 **Curvatures.** Generally speaking, in the differential geometry of  
241 surfaces one considers the *Gauss map*  $\sigma$  from a surface  $S$  to a con-  
242 vex unit sphere  $\Phi$  by requiring that corresponding points have par-  
243 allel tangent planes. Subsequently mean curvature  $H^{\text{rel}}$  and Gaus-  
244 sian curvature  $K^{\text{rel}}$  relative to  $\Phi$  are computed from the derivative  
245  $d\sigma$ . Classically  $\Phi$  is the ordinary unit sphere  $x^2 + y^2 + z^2 = 1$ , so  
246 that  $\sigma$  maps each point to its unit normal vector.

247 In our setting, parallelity is a property of *points* rather than planes,  
248 and the Gauss map  $\sigma$  goes the other way, mapping the tangent

planes of the unit sphere  $z = \phi(x, y)$  to the corresponding tangent plane of the surface  $z = s(x, y)$ . If we know which point a plane is attached to, then the Gauss map is determined by the plane's gradient. So we simply write

$$\nabla\phi \xrightarrow{\sigma} \nabla s.$$

By moving along a curve  $\mathbf{u}(t) = (x(t), y(t))$  in the parameter domain we get the first variation of tangent planes:  $\frac{d}{dt}\nabla\phi|_{\mathbf{u}(t)} = (\nabla^2\phi)\dot{\mathbf{u}}$ . This yields the derivative  $(\nabla^2\phi)\dot{\mathbf{u}} \xrightarrow{d\sigma} (\nabla^2s)\dot{\mathbf{u}}$ , for all  $\dot{\mathbf{u}}$ , and the matrix of  $d\sigma$  is found as  $(\nabla^2\phi)^{-1}(\nabla^2s)$ . By definition, curvatures of the surface  $s$  relative to  $\phi$  are found as

$$K_s^{\text{rel}} = \det(d\sigma) = \frac{\det\nabla^2s}{\det\nabla^2\phi},$$

$$H_s^{\text{rel}} = \frac{1}{2}\text{tr}(d\sigma) = \frac{1}{2}\text{tr}\left(\frac{M}{\det\nabla^2\phi}\nabla^2s\right) = \frac{\Delta_\phi s}{2\det\nabla^2\phi}.$$

The Maxwell paraboloid  $\phi_0(x, y) = \frac{1}{2}(x^2 + y^2)$  is the canonical unit sphere of isotropic geometry, with Hessian  $E_2$ . Curvatures relative to  $\phi_0$  are not called "relative" and are denoted by the symbols  $H, K$  instead of  $H^{\text{rel}}, K^{\text{rel}}$ . The observation

$$\Delta_\phi\phi = \text{tr}(M\nabla^2\phi) = \text{tr}(\widehat{\nabla^2\phi}\nabla^2\phi) = 2\det\nabla^2\phi$$

together with the formulas above implies

$$K_s = \det\nabla^2s, K_\phi = \det\nabla^2\phi \implies H_s^{\text{rel}} = \frac{\Delta_\phi s}{2K_\phi} = \frac{\Delta_\phi s}{\Delta_\phi\phi}.$$

**Relation to Self-supporting Surfaces.** Summarizing the formulas above, we rewrite the balance condition (1) as

$$2K_\phi H_s^{\text{rel}} = \Delta_\phi s = F. \quad (4)$$

Let us draw some conclusions:

- Since  $H_\phi^{\text{rel}} = 1$  we see that the load  $F_\phi = 2K_\phi$  is admissible for the stress surface  $\phi(x, y)$ , which is hereby shown as self-supporting. The quotient of loads yields  $H_s^{\text{rel}} = F/F_\phi$ .
- If the stress surface coincides with the Maxwell paraboloid, then *constant loads characterize constant mean curvature surfaces*, because we get  $K_\phi = 1$  and  $H_s = F/2$ .
- If  $s_1, s_2$  have the same stress potential  $\phi$ , then  $H_{s_1-s_2}^{\text{rel}} = H_{s_1}^{\text{rel}} - H_{s_2}^{\text{rel}} = 0$ , so  $s_1 - s_2$  is a (relative) minimal surface.

## 2.4 Meshes in Isotropic Geometry

A general theory of curvatures of polyhedral surfaces with respect to a polyhedral unit sphere was proposed by [Pottmann et al. 2007; Bobenko et al. 2010], and its dual complement in isotropic geometry was elaborated on in [Pottmann and Liu 2007]. As illustrated by Figure 4, the mean curvature of a self-supporting surface  $\mathcal{S}$  relative to its discrete Airy stress potential is associated with the vertices of  $\mathcal{S}$ . It is computed from areas and mixed areas of faces in the polar polyhedra  $\mathcal{S}^*$  and  $\Phi^*$ :

$$H^{\text{rel}}(\mathbf{v}_i) = \frac{A_i(\mathcal{S}, \Phi)}{A_i(\Phi, \Phi)}, \quad \text{where}$$

$$A_i(\mathcal{S}, \Phi) = \frac{1}{4} \sum_{k: f_k \in 1\text{-ring}(\mathbf{v}_i)} \det(\mathbf{v}'_k, \mathbf{w}'_{k+1}) + \det(\mathbf{w}'_k, \mathbf{v}'_{k+1}).$$

The prime denotes the projection into the  $xy$  plane, and summation is over those dual vertices which are adjacent to  $\mathbf{v}_i$ . Replacing  $\mathbf{v}'_k$  by  $\mathbf{w}'_k$  yields  $A_i(\Phi, \Phi) = \frac{1}{2} \sum \det(\mathbf{w}'_k, \mathbf{w}'_{k+1})$ .

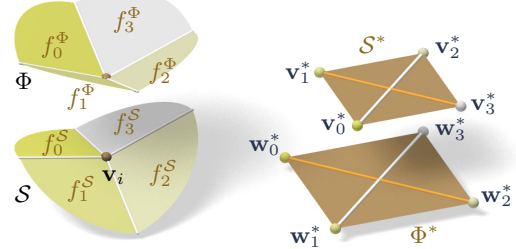


**Figure 4:** Mean curvature of a vertex  $\mathbf{v}_i$  of  $\mathcal{S}$ : Corresponding edges of the polar duals  $\mathcal{S}^*$ ,  $\Phi^*$  are parallel, and mean curvature according to [Pottmann et al. 2007] is computed from the vertices polar to faces adjacent to  $\mathbf{v}_i$ . For valence 4 vertices the case of zero mean curvature shown here is characterized by parallelity of non-corresponding diagonals of corresponding quads in  $\mathcal{S}^*$ ,  $\Phi^*$ .

**Proposition.** If  $\Phi$  is the Airy surface of a thrust network  $\mathcal{S}$ , then the mean curvature of  $\mathcal{S}$  relative to  $\Phi$  is computable as

$$H^{\text{rel}}(\mathbf{v}_i) = \frac{\sum_{j \sim i} w_{ij}(s_j - s_i)}{\sum_{j \sim i} w_{ij}(\phi_j - \phi_i)} = \frac{\Delta_\phi s}{\Delta_\phi\phi}|_{\mathbf{v}_i}. \quad (5)$$

**Proof.** It is sufficient to show  $2A_i(\mathcal{S}, \Phi) = \sum_{j \sim i} w_{ij}(s_j - s_i)$ .

For that, consider edges  $\mathbf{e}'_1, \dots, \mathbf{e}'_n$  emanating from  $\mathbf{v}'_i$ . The dual cycles in  $\Phi^{*\prime}$  and  $\mathcal{S}^{*\prime}$  without loss of generality are given by vertices  $(\mathbf{v}'_1, \dots, \mathbf{v}'_n)$  and  $(\mathbf{w}'_1, \dots, \mathbf{w}'_n)$ , respectively. The latter has edges  $\mathbf{w}'_{j+1} - \mathbf{w}'_j = w_{ij}J\mathbf{e}'_j$  (indices modulo  $n$ ).

Without loss of generality  $\mathbf{v}_i = 0$ , so the vertex  $\mathbf{v}'_j$  by construction equals the gradient of the linear function  $\mathbf{x} \mapsto \langle \mathbf{v}'_j, \mathbf{x} \rangle$  defined by the properties  $\mathbf{e}'_{j-1} \mapsto s_{j-1} - s_i, \mathbf{e}'_j \mapsto s_j - s_i$ . Corresponding edge vectors  $\mathbf{v}'_{j+1} - \mathbf{v}'_j$  and  $\mathbf{w}'_{j+1} - \mathbf{w}'_j$  are parallel, because  $\langle \mathbf{v}'_{j+1} - \mathbf{v}'_j, \mathbf{e}'_j \rangle = (s_j - s_i) - (s_j - s_i) = 0$ . Expand  $2A_i(\mathcal{S}, \Phi)$ :

$$\begin{aligned} & \frac{1}{2} \sum \det(\mathbf{w}'_j, \mathbf{v}'_{j+1}) + \det(\mathbf{v}'_j, \mathbf{w}'_{j+1}) \\ &= \frac{1}{2} \sum \det(\mathbf{w}'_j - \mathbf{w}'_{j+1}, \mathbf{v}'_{j+1}) + \det(\mathbf{v}'_j, \mathbf{w}'_{j+1} - \mathbf{w}'_j) \\ &= \frac{1}{2} \sum \det(-w_{ij}J\mathbf{e}'_j, \mathbf{v}'_{j+1}) + \det(\mathbf{v}'_j, w_{ij}J\mathbf{e}'_j) \\ &= \sum \det(\mathbf{v}'_j, w_{ij}J\mathbf{e}'_j) = \sum w_{ij} \langle \mathbf{v}'_j, \mathbf{e}'_j \rangle = \sum w_{ij}(s_j - s_i). \end{aligned}$$

Here we have used  $\det(\mathbf{a}, J\mathbf{b}) = \langle \mathbf{a}, \mathbf{b} \rangle$ .  $\square$

In order to discretize (4), we also need a discrete Gaussian curvature, usually defined as a quotient of areas which correspond under the Gauss mapping. We define

$$K_\Phi(\mathbf{v}_i) = \frac{A_i(\Phi, \Phi)}{A_i},$$

where  $A_i$  is the Voronoi area of vertex  $\mathbf{v}'_i$  in the projected mesh  $\mathcal{S}'$  used in (3).

**Remark:** If the faces of the thrust network  $\mathcal{S}$  are not planar, the simple trick of introducing additional edges with zero forces in them makes them planar, and the theory is applicable. In the interest of space, we refrain from elaborating further.

**Discrete Balance Equation.** The discrete version of the balance equation (4) reads as follows:

**Theorem.** A simply-connected mesh  $\mathcal{S}$  with vertices  $\mathbf{v}_i = (x_i, y_i, s_i)$  can be put into static equilibrium with vertical nodal forces  $A_i F_i$  if and only if there exists a combinatorially equivalent

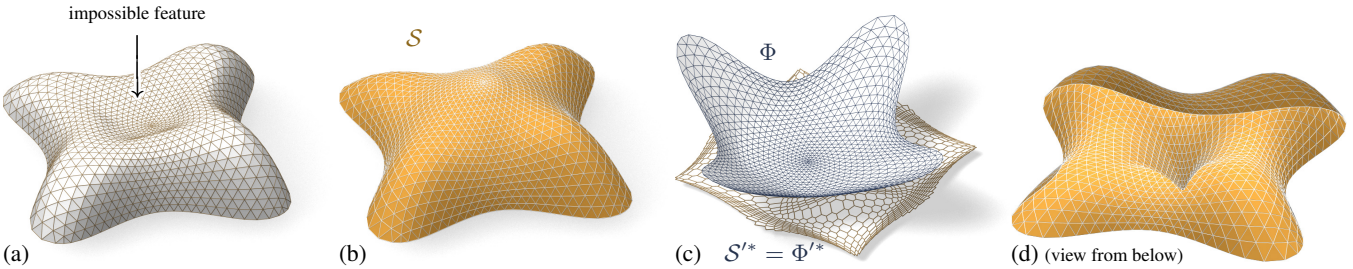


**Figure 5:** The top of the Lilium Tower (a) cannot stand as a masonry structure, because its central part is concave. Our algorithm finds a nearby self-supporting mesh (b) without this impossible feature. (c) shows the corresponding Airy mesh  $\Phi$  and reciprocal force diagram  $S'^*$ . (d) The user can edit the original surface, such as by specifying that the center of the surface is supported by a vertical pillar, and the self-supporting network adjusts accordingly.

313 mesh  $\Phi$  with planar faces and vertices  $(x_i, y_i, \phi_i)$ , such that cur-  
314 vatures of  $\mathcal{S}$  relative to  $\Phi$  obey

$$2K_\Phi(\mathbf{v}_i)H^{\text{rel}}(\mathbf{v}_i) = F_i \quad (6)$$

315 at every interior vertex and every free boundary vertex  $\mathbf{v}_i$ .  $\mathcal{S}$  can  
316 be put into compressive static equilibrium if and only if there exists  
317 a convex such  $\Phi$ .

318 *Proof.* The relation between equilibrium forces  $w_{ij}\mathbf{e}_{ij}$  in  $\mathcal{S}$  and  
319 the polyhedral stress potential  $\Phi$  has been discussed above, and  
320 so has the equivalence “ $w_{ij} \geq 0 \iff \Phi$  convex” (see e.g.  
321 [Ash et al. 1988] for a survey of this and related results). It re-  
322 mains to show that Equations (2) and (6) are equivalent. This is  
323 the case because the proposition above implies  $2K(\mathbf{v}_i)H^{\text{rel}}(\mathbf{v}_i) =$   
324  $2 \frac{A_i(\Phi, \Phi)}{A_i} \frac{A_i(\Phi, \mathcal{S})}{A_i(\Phi, \Phi)} = \frac{1}{A_i} (\sum_{j \sim i} w_{ij}(s_j - s_i)) = \frac{1}{A_i} A_i F_i$ .  $\square$

## 325 2.5 Convergence.

326 When considering discrete thrust networks as discretizations of  
327 continuous self-supporting surfaces, the following question is im-  
328 portant: For a given smooth surface  $s(x, y)$  with stress potential  $\phi$ ,  
329 does there exist a polyhedral surface  $\mathcal{S}$  in equilibrium approximat-  
330 ing  $s(x, y)$ , whose top view is a given planar mesh  $\mathcal{S}'$ ? We restrict  
331 our attention to triangle meshes, where planarity of the faces of the  
332 discrete stress surface  $\Phi$  is not an issue. Equivalently, we ask:

- 333 • Does  $\mathcal{S}'$  have a reciprocal diagram whose corresponding Airy  
334 polyhedron  $\Phi$  approximates the continuous Airy potential  $\phi$ ?  
335 (if the surfaces involved are not simply connected, these ob-  
336 jects are defined locally).
- 337 • Does  $\mathcal{S}'$  possess a “perfect” discrete Laplace-Beltrami opera-  
338 tor  $\Delta_\phi$  in the sense of Wardetzky et al. [2007] whose weights  
339 are the edge length scalars of such a reciprocal diagram?

340 From [Wardetzky et al. 2007] we know that perfect Laplacians ex-  
341 ist only on regular triangulations which are projections of convex  
342 polyhedra. On the other hand, previous sections show how to ap-  
343 propriately re-triangulate: Let  $\Phi$  be a triangle mesh convex hull of  
344 the vertices  $(x_i, y_i, \phi(x_i, y_i))$ , where  $(x_i, y_i)$  are vertices of  $\mathcal{S}'$ .  
345 Then its polar dual  $\Phi^*$  projects onto a reciprocal diagram with pos-  
346 itive edge weights, so  $\Delta_\phi$  has positive weights, and the vertices  
347  $(x_i, y_i, s_i)$  of  $\mathcal{S}$  can be found by solving the discrete Poisson prob-  
348 lem  $(\Delta_\phi s)_i = A_i F_i$ .

349 We expect, but we don’t prove, that the discrete  $\Delta_\phi$  approximates  
350 its continuous counterpart for reasonable sampling (after all it is  
351 directly derived from  $\phi(x, y)$ ). This implies that solving the dis-  
352 crete Poisson equation leads to a mesh approximating its continu-  
353 ous counterpart  $s(x, y)$ , and we have convergence as the sampling  
354 density increases. A rigorous analysis is a topic for future research.

## 355 3 Thrust Networks from Reference Meshes

356 Consider now the problem of taking a given reference mesh, say  
357  $\mathcal{R}$ , and finding a combinatorially equivalent mesh  $\mathcal{S}$  in static equi-  
358 librium approximating  $\mathcal{R}$ . The loads on  $\mathcal{S}$  include user-prescribed  
359 loads as well as the dead load caused by the mesh’s own weight.  
360 Conceptually, finding  $\mathcal{S}$  amounts to minimizing some formulation  
361 of distance between  $\mathcal{R}$  and  $\mathcal{S}$ , subject to constraints (2), (3), and  
362  $w_{ij} \geq 0$ . For any choice of distance this minimization will be a  
363 nonlinear, non-convex, inequality-constrained variational problem.  
364 Our experience with black-box solvers [Wächter and Biegler 2006]  
365 is that they perform well for surfaces without complex geometry or  
366 for polishing reference meshes close to self-supporting, but fail to  
367 converge in reasonable time for more complicated shapes such as  
368 the one of Fig. 1, left. We therefore propose the following special-  
369 ized, staggered linearization for solving the optimization problem:  
370

- 371 0. Start with an initial guess  $\mathcal{S} = \mathcal{R}$ .
- 372 1. Estimate the self-load on the vertices of  $\mathcal{S}$ , using their current  
373 positions.
- 374 2. Fixing  $\mathcal{S}$ , locally fit an associated stress surface  $\Phi$ .
- 375 3. Alter positions  $\mathbf{v}_i$  to improve the fit.
- 376 4. Repeat from Step 1 until convergence.

377 *Remark:* This staggered approach shares several advantages of  
378 solving the full nonlinear problem: a nearby self-supporting sur-  
379 face is found given only a suggested reference shape, without need-  
380 ing to single one of the many possible top view reciprocal diagrams  
381 or needing to specify boundary tractions – these are found automati-  
382 cally during optimization. Although providing an initial top view  
383 graph with good combinatorics remains important, by not fixing the  
384 top view our approach allows the thrust network to slide both ver-  
385 tically and tangentially to the ground, essential to finding faithful  
386 thrust networks for surfaces with free boundary conditions.

387 **Step 1: Estimating Self-Load.** The dead load due to the sur-  
388 face’s own weight depends not only on the top view of  $\mathcal{S}$ , but also  
389 on the surface area of its faces. To avoid adding nonlinearity to  
390 the algorithm, we estimate the load coefficients  $F_i$  at the beginning  
391 of each iteration, and assume they remain constant until the next  
392 iteration. We estimate the load  $A_i F_i$  associated with each vertex  
393 by calculating its Voronoi surface area on each of its incident faces  
394 (note that this surface area is distinct from  $A_i$ , the vertex’s Voronoi  
395 area on the top view), and then multiplying by a user-specified sur-  
396 face density  $\rho$ .

397 **Step 2: Fit a Stress Surface.** In this step, we fix  $\mathcal{S}$  and try to  
398 fit a stress surface  $\Phi$  subordinate to the top view  $\mathcal{S}'$  of the primal  
399 mesh. We do so by searching for dihedral angles between the faces  
400 of  $\Phi$  which minimize, in the least-squares sense, the error in force



**Figure 6:** A freeform surface (left) needs adjustments around the entrance arch and between the two pillars in order to be self-supporting; our algorithm finds the nearby surface in equilibrium (right) that incorporates these changes.

Fig.	Vertices	Edges	Time (s)	Iterations	Max. Rel. Error
5b	1201	3504	21.6	9	$4.2 \times 10^{-5}$
5d	1200	3500	26.5	10	$8.5 \times 10^{-5}$
6	1535	2976	17.0	21	$2.7 \times 10^{-5}$
8	752	2165	8.0	9	$5.8 \times 10^{-5}$
9	2358	4302	19.5	9	$3.0 \times 10^{-4}$
16	527	998	5.7	25	$2.4 \times 10^{-5}$

**Table 1:** Numerical details about our examples. We show the clock time needed by an Intel Xeon 2.3GHz desktop PC with 4 GB of RAM to find a self-supporting thrust network and associated stress surface from the example’s reference mesh; we also give the number of outer iterations of the four steps in (§3). The maximum relative error is the dimensionless quantity  $\max_i \|A_i F_i - \sum_{j \sim i} w_{ij}(\mathbf{v}_j - \mathbf{v}_i)\| / \|A_i F_i\|$  (the maximum is taken over interior vertices  $\mathbf{v}_i$ ).

equilibrium (6) and local integrability of  $\Phi$ . Doing so is equivalent to minimizing the squared residuals of Equations (3) and (2), with the positions held fixed. We define the *equilibrium energy*

$$E = \sum_i \left\| \begin{pmatrix} 0 \\ A_i F_i \end{pmatrix} - \sum_{j \sim i} w_{ij}(\mathbf{v}_j - \mathbf{v}_i) \right\|^2, \quad (7)$$

where  $i$  runs through interior and free boundary vertices, and solve

$$\min_{w_{ij}} E, \quad \text{s.t. } 0 \leq w_{ij} \leq w_{\max}. \quad (8)$$

Here  $w_{\max}$  is an optional maximum weight we are willing to assign (to limit the amount of stress in the surface). This convex, sparse, box-constrained least-squares problem [Friedlander 2007] always has a solution. If the objective is 0 at this solution,  $\mathcal{S}$  is self-supporting – we are done. Otherwise,  $\mathcal{S}$  is not self-supporting and its vertices must be moved.

**Step 3: Alter Positions.** In the previous step we fit as best as possible a stress surface  $\Phi$  to  $\mathcal{S}$ . There are two possible kinds of error with this fit: the faces around a vertex (equivalently, the reciprocal diagram) might not close up; and the resulting stress forces might not be exactly in equilibrium with the loads. These errors can be decreased by modifying the top view and heights of  $\mathcal{S}$ , respectively. It is possible to simply solve for new vertex positions that put  $\mathcal{S}$  in static equilibrium, since Equations (2) and (3) with  $w_{ij}$  fixed form a square linear system that is typically nonsingular.

While this approach would yield a self-supporting  $\mathcal{S}$ , this mesh is often far from the reference mesh  $\mathcal{R}$ , since any local errors in the stress surface from Step 2 amplify into global errors in  $\mathcal{S}$ . We propose instead to look for new positions that decrease the imbalance in the stresses and loads, while also penalizing drift away from the reference mesh:

$$\min_{\mathbf{v}} E + \alpha \sum_i \langle \mathbf{n}_i, \mathbf{v}_i - \mathbf{v}_i^0 \rangle^2 + \beta \|\mathbf{v} - \mathbf{v}_P^0\|^2,$$

where  $\mathbf{v}_i^0$  is the position of the  $i$ -th vertex at the start of this step of the optimization,  $\mathbf{n}_i$  is the starting vertex normal (computed as

the average of the incident face normals),  $\mathbf{v}_P^0$  is the projection of  $\mathbf{v}^0$  onto the reference mesh, and  $\alpha > \beta$  are penalty coefficients that are decreased proportionally to the decrease in  $E$  at every iteration of Steps 1–3. The second term allows  $\mathcal{S}$  to slide over itself (if doing so improves equilibrium) but penalizes drift in the normal direction. The third term, weaker than the second, regularizes the optimization by preventing large drift away from the reference surface or excessive tangential sliding.

**Implementation Details.** Solving the weighted least-squares problem of Step 3 amounts to solving a sparse, symmetric linear system. While the MINRES algorithm [Paige and Saunders 1975] is likely the most robust algorithm for solving this system, in practice we have observed that the method of conjugate gradients works well despite the potential ill-conditioning of the objective matrix.

**Limitations.** This algorithm is not guaranteed to always converge; this fact is not surprising from the physics of the problem (if the boundary of the reference mesh encloses too large of a region,  $w_{\max}$  is set too low, and the density of the surface too high, a thrust network in equilibrium simply does not exist – the vault is too ambitious and cannot be built to stand; pillars are needed.)

We can, however, make a few remarks. Only Step 1 can increase the equilibrium energy  $E$  of Equation (7). Step 2 always decreases it, and Step 3 does as well as  $\beta \rightarrow 0$ . Moreover, as  $\alpha \rightarrow 0$  and  $\beta \rightarrow 0$ , Step 3 approaches a linear system with as many equations as unknowns; if this system has full rank, its solution sets  $E = 0$ . These facts suggest that the algorithm should generally converge to a thrust network in equilibrium, provided that Step 1 does not increase the loads by too much at every iteration, and this is indeed what we observe in practice. One case where this assumption is guaranteed to hold is if the thickness of the surface is allowed to freely vary, so that it can be chosen so that the surface has uniform density over the top view.

If the linear system in Step 3 is singular and infeasible, the algorithm can stall at  $E > 0$ . This failure occurs, for instance, when an interior vertex has height  $z_i$  lower than all of its neighbors, and Step 2 assigns all incident edges to that vertex a weight of zero: clearly no amount of moving the vertex or its neighbors can bring the vertex into equilibrium. We avoid such degenerate configurations by bounding weights slightly away from zero in (8), trading increased robustness for slight smoothing of the resulting surface. Attempting to optimize meshes that have self-intersecting top views (i.e., aren’t height fields), have too many impossible features, or are insufficiently supported by fixed boundary points can also result in errors and instability.

## 4 Results

**Interactive Design of Self-Supporting Surfaces.** The optimization algorithm described in the previous section forms the basis of an interactive design tool for self-supporting surfaces. Users manipulate a mesh representing a reference surface, and the computer searches for a nearby thrust network in equilibrium (see e.g. Figure 7). Features of the design tool include:

- Handle-based 3D editing of the reference mesh using Laplacian coordinates [Lipman et al. 2004; Sorkine et al. 2003] to extrude vaults, insert pillars, and apply other deformations to the reference mesh. Handle-based adjustments of the heights, keeping the top view fixed, and deformation of the top view, keeping the heights fixed, are also supported. The thrust network adjusts interactively to fit the deformed positions, giving the usual visual feedback about the effects of edits on whether

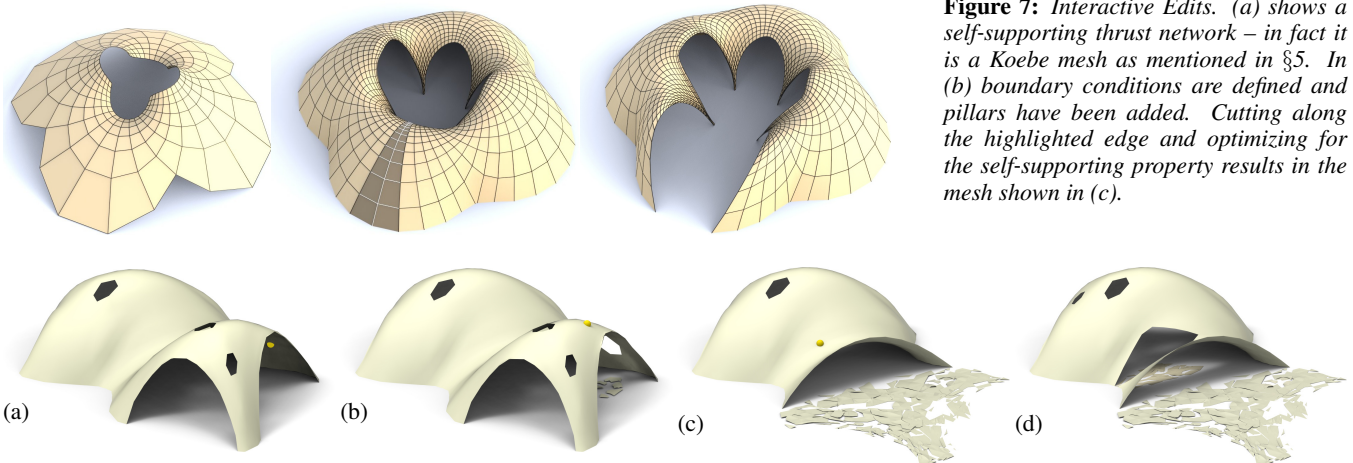


**Figure 8: Destruction sequence.** We simulate removing small parts of masonry (their location is shown by a yellow ball) and the falling off of further pieces which are no longer supported after removal. For this example, removing a certain small number of single bricks does not affect stability (a,b). Removal of material at a certain point (yellow ball in (b)) will cause a greater part of the structure to collapse, as seen in (c). (d) shows the result after one more removal (all images show the respective thrust networks, not the reference surface).

486 or not the surface can stand.

- 487 • Specification of boundary conditions. Points of contact be-  
488 tween the reference surface and the ground or environment  
489 are specified by “pinning” vertices of the surface, specifying  
490 that the thrust network must coincide with the reference mesh  
491 at this point, and relaxing the condition that forces must be in  
492 equilibrium there.
- 493 • Interactive adjustment of surface density  $\rho$ , external loads,  
494 and maximum permissible stress per edge  $w_{\max}$ , with visual  
495 feedback of how these parameters affect the fitted thrust net-  
496 work.
- 497 • Upsampling of the thrust network through Catmull-Clark sub-  
498 division and polishing of the resulting refined thrust network  
499 using optimization (§3).
- 500 • Visualization of the stress surface dual to the thrust network  
501 and corresponding reciprocal diagram.

502 **Examples. Top of the Lilium Tower:** Consider the top portion of the  
503 steel-glass exterior surface of the Lilium Tower, which is currently  
504 being built in Warszaw (see Figure 5). What is if we had wanted to  
505 build this surface out of masonry instead? This surface contains a  
506 concave part with local minimum in its interior and so cannot pos-  
507 sibly be self-supporting without modification. Given this surface as  
508 a reference mesh, our algorithm constructs a nearby thrust network  
509 in equilibrium without the impossible feature. The user can then  
510 explore how editing the reference mesh – adding a pillar, for exam-  
511 ple – affects the thrust network and its deviation from the reference  
512 surface.

513 **Example: Freeform Structure with Two Pillars.** Suppose an archi-  
514 tect’s experience and intuition has permitted the design of a nearly  
515 self-supporting freeform surface (Figure 6). Our algorithm reveals  
516 those edits needed to make the structure sound – principally around  
517 the entrance arch, and the area between the two pillars.

518 **Example: Interactive Editing.** Figure 7 shows an example of the de-  
519 sign and optimization workflow. Starting with a mesh, we first add  
520 pillars in the center and clean up the outer boundary (by fixing it to  
521 the floor). A subsequent cut needs a further round of optimization.  
522 This surface is neither convex nor simply connected, and exhibits a  
523 mix of boundary conditions, none of which cause our algorithm any  
524 difficulty; it always finds a self-supporting thrust network near the  
525 designed reference mesh. The user is free to make edits to the refer-

**Figure 7: Interactive Edits.** (a) shows a self-supporting thrust network – in fact it is a Koebe mesh as mentioned in §5. In (b) boundary conditions are defined and pillars have been added. Cutting along the highlighted edge and optimizing for the self-supporting property results in the mesh shown in (c).

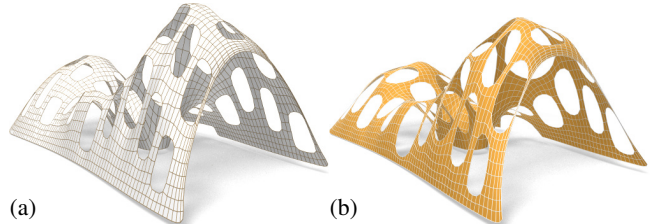


**Figure 9: A mesh with holes (a) requires large deformations to both the top view and heights to render it self-supporting (b)**

526 ence mesh, and the thrust network adapts to these edits, providing  
527 the user feedback on whether these designs are physically realizable  
528 [we refer to the accompanying video for interactive building  
529 and editing of freeform self-supporting shapes].

530 **Example: Destruction Sequence.** In Figure 8 we simulate removing  
531 parts of masonry and the falling off of further pieces which are no  
532 longer supported after removal. This is done by deleting the 1-  
533 neighborhood of a vertex and solving for a new thrust network in  
534 compressive equilibrium close to the original reference surface. We  
535 delete those parts of the network which deviate too much and are  
536 no longer contained in the masonry hull, and iterate.

537 **Example: Swiss Cheese.** Cutting holes in a self-supporting surface  
538 interrupts force flow lines and causes dramatic global changes to  
539 the surface stresses, often to the point that the surface is no longer  
540 in equilibrium. Whether a given surface with many such holes can  
541 stand is far from obvious. Figure 9a shows such an implausible and  
542 unstable surface; our optimization finds a nearby, equally implau-  
543 sible but stable surface without difficulty (see Figures 1, left and  
544 9b).

545 **Example: Stability Test:** See Figures 10 and 11 for a series of im-  
546 ages which visualize the effect of additional loads on a thrust net-  
547 work.

548 **Example: Structural Glass.** See Figure 16 for details on a self-  
549 supporting surface which is realized not as masonry, but as a steel/  
550 glass construction with glass as a structural element.

**Figure 10:** Stability Test. Left: Coloring and cross-section of edges visualize the magnitude of forces in a thrust network which is in equilibrium with this dome’s dead load. Right: When an additional load is applied, there exists a corresponding compressive thrust network which is still contained in the masonry hull of the original dome. This implies stability of the dome under that load.

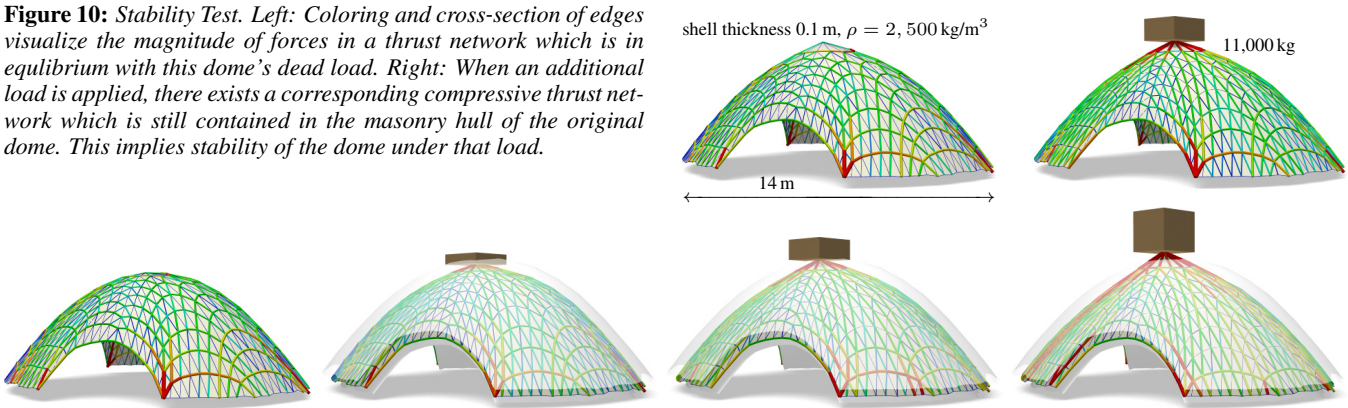


**Figure 11:** Stability test similar to Figure 10, but with a shell thickness of 1 m, in order to better visualize the way the thrust network starts to leave the masonry hull as the load increases. Additional loads are 0 kg, 5,000 kg, 10,000 kg, and 20,000 kg, resp., from left to right.

## 5 Special Self-Supporting Surfaces

**PQ Meshes.** Meshes with *planar* faces are of particular interest in architecture, so in this section we discuss how to remesh a given thrust network in equilibrium such that it becomes a quad mesh with planar faces (again in equilibrium). If this mesh is realized as a steel-glass construction, it is self-supporting in its beams alone, with no forces exerted on the glass (this is the usual manner of using glass). The beams constitute a self-supporting structure which is in perfect force equilibrium (without moments in the nodes) if only the deadload is applied.

Taking an arbitrary non-planar quad mesh and attempting naive, simultaneous enforcement of planarity and static equilibrium – either by staggering a planarity optimization step every outer iteration, or adding a planarity penalty term to the position update – does not yield good results, as shown in Figure 12. Indeed, as we will see later in this section, such a planar perturbation of a thrust network is not expected to generally exist.

Consider a planar quad mesh  $\mathcal{S}$  with vertices  $\mathbf{v}_{ij} = (x_{ij}, y_{ij}, s_{ij})$  which approximates a given continuous surface  $s(x, y)$ . It is known that  $\mathcal{S}$  must approximately follow a network of conjugate curves in the surface (see e.g. [Liu et al. 2006]). We can derive this condition in an elementary way as follows: Using a Taylor expansion, we compute the volume of the convex hull of the quadrilateral  $\mathbf{v}_{ij}, \mathbf{v}_{i+1,j}, \mathbf{v}_{i+1,j+1}, \mathbf{v}_{i,j+1}$ , assuming the vertices lie exactly on the surface  $s(x, y)$ . This results in

$$\text{vol} = \frac{1}{6} \det(\mathbf{a}_1, \mathbf{a}_2) \cdot ((\mathbf{a}_1)^T \nabla^2 s \mathbf{a}_2) + \dots,$$

where  $\mathbf{a}_1 = \begin{pmatrix} x_{i+1,j} - x_{ij} \\ y_{i+1,j} - y_{ij} \end{pmatrix}$ ,  $\mathbf{a}_2 = \begin{pmatrix} x_{i,j+1} - x_{ij} \\ y_{i,j+1} - y_{ij} \end{pmatrix}$ ,

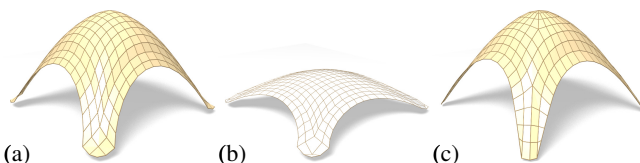


**Figure 12:** Directly enforcing planarity of the faces of even a very simple self-supporting quad-mesh vault (a) results in a surface far removed from the original design (b). Starting instead from a remeshing of the surface with edges following relative principal curvature directions yields a self-supporting, PQ mesh far more faithful to the original (c).

and the dots indicate higher order terms. We see that planarity requires  $(\mathbf{a}_1)^T \nabla^2 s \mathbf{a}_2 = 0$ . In addition to the mesh  $\mathcal{S}$  approximating the surface  $s(x, y)$ , the corresponding polyhedral Airy surface  $\Phi$  must approximate  $\phi(x, y)$ ; thus we get the conditions

$$(\mathbf{a}_1)^T \nabla^2 s \mathbf{a}_2 = (\mathbf{a}_1)^T \nabla^2 \phi \mathbf{a}_2 = 0.$$

$\mathbf{a}_1, \mathbf{a}_2$  are therefore eigenvectors of  $(\nabla^2 \phi)^{-1} \nabla^2 s$ . In view of §2.3,  $\mathbf{a}_1, \mathbf{a}_2$  indicate the principal directions of the surface  $s(x, y)$  relative to  $\phi(x, y)$ .

In the discrete case, where  $s, \phi$  are not given as continuous surfaces, but are represented by a mesh in equilibrium and its Airy mesh, we use the techniques of Schiftner [2007] and Cohen-Steiner and Morvan [2003] to approximate the Hessians  $\nabla^2 s, \nabla^2 \phi$ , compute principal directions as eigenvectors of  $(\nabla^2 \phi)^{-1} \nabla^2 s$ , and subsequently find meshes  $\mathcal{S}, \Phi$  approximating  $s, \phi$  which follow those directions. Global optimization can now polish  $\mathcal{S}, \Phi$  to a valid thrust network with discrete stress potential, where before it failed: we do so by taking the planarity energy  $\sum_f (2\pi - \theta_f)^2$ , where the sum runs over faces and  $\theta_f$  is the sum of the interior angles of face  $f$ , linearizing it at every iteration, and adding it to the objective function of the position update (Step 3). Convexity of  $\Phi$  ensures that  $\mathcal{S}$  is self-supporting.

Note that for each  $\Phi$ , the relative principal curvature directions give the *unique* curve network along which a planar quad discretization of a self-supporting surface is possible. Other networks lead to results like the one shown by Figure 12. Figures 13 and 14 further illustrate the result of applying this procedure to self-supporting surfaces.

**Remark:** When remeshing a given shape by planar quad meshes, we know that the circular and conical properties require that the mesh follows the ordinary, Euclidean principal curvature directions [Liu et al. 2006]. It is remarkable that the self-supporting property in a similar manner requires us to follow certain *relative* principal directions. Practitioners’ observations regarding the beneficial statics properties of principal directions can be explained by this analogy, because the relative principal directions are close to the Euclidean ones, if the stress distribution is uniform and  $\|\nabla s\|$  is small.

**Koenigs Meshes.** Given a self-supporting thrust network  $\mathcal{S}$  with stress surface  $\Phi$ , we ask the question: Which vertical perturbation  $\mathcal{S} + \mathcal{R}$  is self-supporting, with the same loads as  $\mathcal{S}$ ? As to notation, all involved meshes  $\mathcal{S}, \mathcal{R}, \Phi$  have the same top view, and arithmetic operations refer to the respective  $z$  coordinates  $s_i, r_i, \phi_i$  of vertices.

**Figure 13:** Planar quad remeshing of the surface of Fig. 5. (a) Relative principal directions, found from eigenvectors of  $(\nabla^2\phi)^{-1}\nabla^2s$ . (b) Quad mesh guided by principal directions is almost planar and almost self-supporting. (c) Small changes achieve both properties.

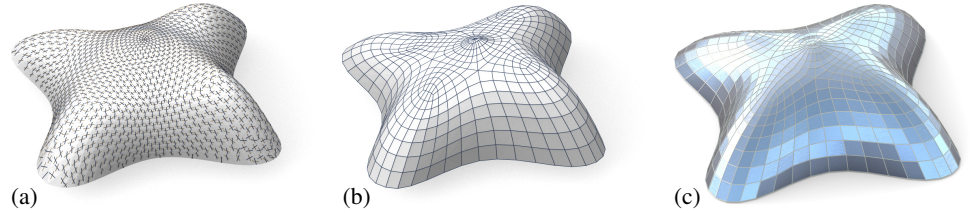


**Figure 14:** Planar quad remeshing of the surface of Figure 6. Left: Relative principal directions. Right: The result of optimization is a self-supporting PQ mesh, which guides a moment-free steel/glass construction (interior view, see also Fig. 1).



616 The condition of equal loads then is expressed as  $\Delta_\phi(s + r) =$   
 617  $\Delta_\phi s$  in terms of Laplacians or as  $H_S^{\text{rel}} = H_{S+\mathcal{R}}^{\text{rel}}$  in terms of mean  
 618 curvature, and is equivalent to

$$\Delta_\phi r = 0, \quad \text{i.e.,} \quad H_{\mathcal{R}}^{\text{rel}} = 0.$$

619 So  $\mathcal{R}$  is a *minimal surface* relative to  $\Phi$ . While in the triangle mesh  
 620 case there are enough degrees of freedom for nontrivial solutions,  
 621 the case of planar quad meshes is more intricate: Polar polyhedra  
 622  $\mathcal{R}^*$ ,  $\Phi^*$  have to be Christoffel duals of each other [Pottmann and  
 623 Liu 2007], as illustrated by Figure 4. Unfortunately not all quad  
 624 meshes have such a dual; the condition is that the mesh is *Koenigs*,  
 625 i.e., the derived mesh formed by the intersection points of diagonals  
 626 of faces again has planar faces [Bobenko and Suris 2008].

## 6 Conclusion and Future Work

636 **Conclusion.** This paper builds on relations between statics and  
 637 geometry, some of which have been known for a long time, and  
 638 connects them with newer methods of discrete differential geometry,  
 639 such as discrete Laplace operators and curvatures of polyhedral  
 640 surfaces. We were able to find efficient ways of modeling self-  
 641 supporting freeform shapes, and provide architects and engineers  
 642 with an interactive tool for evaluating the statics of freeform ge-  
 643 omtries. The self-supporting property of a shape is directly rele-  
 644 vant for freeform masonry. The actual thrust networks we use for  
 645 computation are relevant e.g. for steel constructions, where equili-  
 646 brium of deadload forces implies absence of moments. This theory  
 647 and accompanying algorithms thus constitute a new contribution to  
 648 architectural geometry, connecting statics and geometric design.

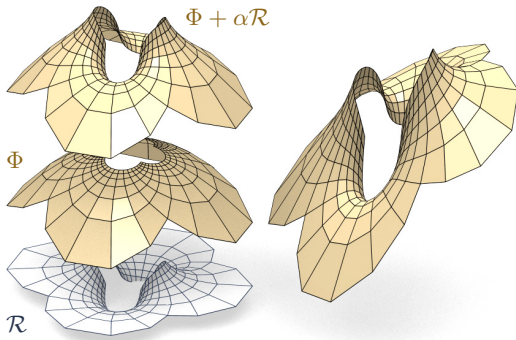


**Figure 15:** Left: A “Koebe” mesh  $\Phi$  is self-supporting for unit dead load. An entire family of self-supporting meshes with the same top view is defined by  $S_\alpha = \Phi + \alpha\mathcal{R}$ , where  $\mathcal{R}$  is chosen as  $\Phi$ ’s Christoffel-dual. The right hand image shows a different example of the same connectivity.

649 **Real-World Examples.** This work was very much inspired by  
 650 Philippe Block’s plenary lecture at the 2011 Symposium on Geom-  
 651 etry Processing in Lausanne. Several illustrations (the destruction  
 652 sequence of Fig. 8 and the maximum load example of Fig. 10) have  
 653 real-world analogues on his web page at ETH Zurich.

654 **Future Work.** There are several directions of future research. One  
 655 is to incorporate non-manifold meshes, which occur naturally when  
 656 e.g. supporting walls are introduced. It is also obvious that non-ver-  
 657 tical loads, e.g. wind load, play a role. There are also some direc-  
 658 tions to pursue in improving the algorithms, for instance adaptive  
 659 remeshing in problem areas. Probably the interesting connections  
 660 between statics and geometry are not yet exhausted: on the one  
 661 hand we expect that interesting new geometry arises from ques-  
 662 tions of statics, on the other hand we would like to propose the  
 663 *geometrization* of problems as a general solution paradigm.

## References

- 664 ANDREU, A., GIL, L., AND ROCA, P. 2007. Computational anal-  
 665 ysis of masonry structures with a funicular model. *J. Engng.  
 666 Mechanics* 133, 473-480.
- 668 ASH, P., BOLKER, E., CRAPO, H., AND WHITELEY, W. 1988.  
 669 Convex polyhedra, Dirichlet tessellations, and spider webs. In  
 670 *Shaping space (Northampton 1984)*. Birkhäuser, 231–250.
- 671 BARNES, M. R. 2009. Form finding and analysis of tension struc-  
 672 tures by dynamic relaxation. *Int. J. Space Struct.* 14, 2, 89–104.

627 **Koebe meshes.** An interesting special case occurs if  $\Phi$  is a  
 628 *Koebe* mesh of isotropic geometry, i.e., a PQ mesh whose edges  
 629 touch the Maxwell paraboloid. Since  $\Phi$  approximates the Maxwell  
 630 paraboloid, we get  $2K(\mathbf{v}_i)H^{\text{rel}}(\mathbf{v}_i) \approx 1$  and  $\Phi$  consequently is  
 631 self-supporting for unit load. Applying the Christoffel dual con-  
 632 struction described above yields a minimal mesh  $\mathcal{R}$  and a family of  
 633 meshes  $\Phi + \alpha\mathcal{R}$  which are self-supporting for unit load (see Fig-  
 634 ure 15).

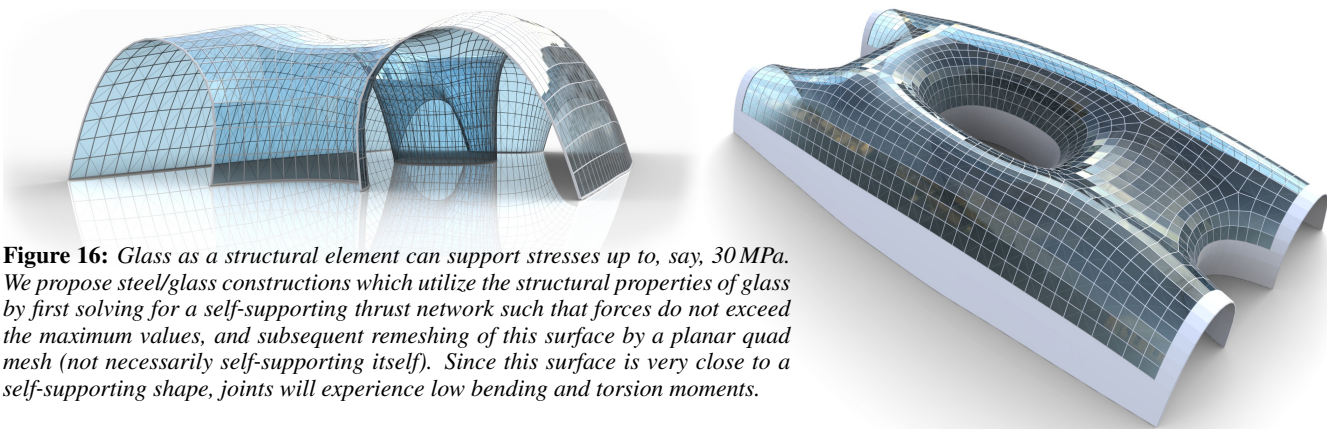


**Figure 16:** Glass as a structural element can support stresses up to, say, 30 MPa. We propose steel/glass constructions which utilize the structural properties of glass by first solving for a self-supporting thrust network such that forces do not exceed the maximum values, and subsequent remeshing of this surface by a planar quad mesh (not necessarily self-supporting itself). Since this surface is very close to a self-supporting shape, joints will experience low bending and torsion moments.

- 673 BLOCK, P., AND LACHAUER, L. 2011. Closest-fit, compression- 713  
674 only solutions for free form shells. In *IABSE — IASS 2011 Lon- 714  
675 don Symposium*, Int. Ass. Shell Spatial Structures. electronic. 715
- 676 BLOCK, P., AND OCHSENDORF, J. 2007. Thrust network analysis: 716  
677 A new methodology for three-dimensional equilibrium. *J. Int. 717  
678 Assoc. Shell and Spatial Structures* 48, 3, 167–173. 718
- 679 BLOCK, P. 2009. *Thrust Network Analysis: Exploring Three- 719  
680 dimensional Equilibrium*. PhD thesis, Massachusetts Institute 720  
681 of Technology. 721
- 682 BLOCK, P., 2011. Project webpage at <http://block.arch.ethz.ch/projects/freeform-catalan-thin-tile-vaulting>. 722  
683
- 684 BOBENKO, A., AND SURIS, YU. 2008. *Discrete differential geo- 724  
685 metry: Integrable Structure*. American Math. Soc. 725
- 686 BOBENKO, A., POTTMANN, H., AND WALLNER, J. 2010. A 726  
687 curvature theory for discrete surfaces based on mesh parallelity. 727  
688 *Math. Annalen* 348, 1–24. 728
- 689 COHEN-STEINER, D., AND MORVAN, J.-M. 2003. Restricted 729  
690 Delaunay triangulations and normal cycle. In *Proc. 19th Symp. 730  
691 Computational Geometry*, ACM, 312–321.
- 692 FRATERNALI, F., ANGELILLO, M., AND FORTUNATO, A. 2002. 731  
693 A lumped stress method for plane elastic problems and the 732  
694 discrete-continuum approximation. *Int. J. Solids Struct.* 39, 733  
695 6211–6240.
- 696 FRATERNALI, F. 2010. A thrust network approach to the equi- 734  
697 librium problem of unreinforced masonry vaults via polyhedral 735  
698 stress functions. *Mechanics Res. Comm.* 37, 2, 198 – 204. 736
- 699 FRIEDLANDER, M. P., 2007. BCLS: Bound constrained least 737  
700 squares. <http://www.cs.ubc.ca/~mpf/bcls>.
- 701 GIAQUINTA, M., AND GIUSTI, E. 1985. Researches on the equi- 738  
702 librium of masonry structures. *Archive for Rational Mechanics 739  
703 and Analysis* 88, 4, 359–392.
- 704 HEYMAN, J. 1966. The stone skeleton. *Int. J. Solids Structures* 2, 740  
705 249–279.
- 706 HEYMAN, J. 1995. *The Stone Skeleton: Structural Engineering of 741  
707 Masonry Architecture*. Cambridge University Press.
- 708 HEYMAN, J. 1998. *Structural Analysis: A Historical Approach*. 742  
709 Cambridge University Press.
- 710 KILIAN, A., AND OCHSENDORF, J. 2005. Particle-spring sys- 743  
711 tems for structural form finding. *J. Int. Assoc. Shell and Spatial 744  
712 Structures* 46, 77–84.
- 713 LIPMAN, Y., SORKINE, O., COHEN-OR, D., LEVIN, D., ROSSI, 714  
715 C., AND SEIDEL, H. 2004. Differential coordinates for interac-  
tive mesh editing. In *Proc. SMI*. IEEE, 181–190.
- 716 LIU, Y., POTTMANN, H., WALLNER, J., YANG, Y.-L., AND 717  
718 WANG, W. 2006. Geometric modeling with conical meshes 719  
720 and developable surfaces. *ACM Trans. Graphics* 25, 3, 681–689.
- 721 LIVESLEY, R. K. 1992. A computational model for the limit anal- 722  
723 ysis of three-dimensional masonry structures. *Meccanica* 27, 161–172.
- 724 MAXWELL, J. 1864. On reciprocal diagrams and diagrams of 725  
726 forces. *Philosophical Magazine* 4, 27, 250–261.
- 727 O'Dwyer, D. 1998. Funicular analysis of masonry vaults. *Com- 728  
729 puters and Structures* 73, 187–197.
- 730 PAIGE, C. C., AND SAUNDERS, M. A. 1975. Solution of sparse 731  
732 indefinite systems of linear equations. *SIAM J. Num. Analysis* 12, 617–629.
- 733 POTTMANN, H., AND LIU, Y. 2007. Discrete surfaces in isotropic 734  
735 geometry. In *Mathematics of Surfaces XII*. Springer, 341–363.
- 736 POTTMANN, H., LIU, Y., WALLNER, J., BOBENKO, A., AND 737  
738 WANG, W. 2007. Geometry of multi-layer freeform structures 739  
740 for architecture. *ACM Trans. Graphics* 26, 3, #65,1–11.
- 741 SCHIFTNER, A., AND BALZER, J. 2010. Statics-sensitive layout 742  
743 of planar quadrilateral meshes. In *Advances in Architectural Ge- 744  
745 ometry 2010*, C. Ceccato et al., Eds. Springer, Vienna, 221–236.
- 746 SCHIFTNER, A. 2007. *Planar quad meshes from relative principal 747  
748 curvature lines*. Master's thesis, TU Wien.
- 749 SORKINE, O., COHEN-OR, D., AND TOLEDO, S. 2003. High- 750  
751 pass quantization for mesh encoding. In *Symposium Geometry 752  
753 processing*. 42–51.
- 754 VAN MELE, T., AND BLOCK, P. 2011. A novel form finding 755  
756 method for fabric formwork for concrete shells. *J. Int. Assoc. 757  
758 Shell and Spatial Structures* 52, 217–224.
- 759 WÄCHTER, A., AND BIEGLER, L. T. 2006. On the implementa- 760  
761 tion of a primal-dual interior point filter line search algorithm for 762  
763 large-scale nonlinear programming. *Math. Progr.* 106, 25–57.
- 764 WARDETZKY, M., MATHUR, S., KÄLBERER, F., AND GRIN- 765  
766 SPUN, E. 2007. Discrete Laplace operators: No free lunch. 767  
768 In *Symposium on Geometry Processing*. 33–37.
- 769 WHITING, E., OCHSENDORF, J., AND DURAND, F. 2009. Proce- 770  
771 dural modeling of structurally-sound masonry buildings. *ACM 772  
773 Trans. Graphics* 28, 5, #112,1–9.